JOURNAL OF CATALYSIS 62, 316–328 (1980)

# Raman Spectra of Pyridine Adsorbed on a Series of X Zeolites

A. H. HARDIN[1], M. KLEMES, AND B. A. MORROW

*Department of Chemistry, University of Ottawa, Ottawa, Ontario, Canada*

Received April 3, 1979; revised August 23, 1979

The adsorption of pyridine on a sodium 13X zeolite and on 10 exchanged X zeolites has been studied by Raman spectroscopy. The band position of the pyridine $\nu_1$ symmetric ring breathing mode (near 991 $cm^{-1}$ for liquid pyridine) shifted linearly to higher frequency as a function of the electrostatic potential ($e/r$) induced by the charge balancing cation, and a similar linear correlation was found for this mode in the spectrum of some metal nitrate–pyridine–nitromethane solutions. We postulate that in both systems the lone pair electrons of pyridine interact directly with the positively charged cation, an interpretation which conforms with other literature results with respect to the infrared and Raman spectra of pyridine adsorbed on other zeolites. In addition, where there was residual unexchanged $Na^+$, an aditional $\nu_1$ band was observed which was assigned to a $Na^+$–pyridine interaction and we have concluded that where ionic size is not a consideration, the exchange cations (both monovalent and bivalent) are distributed at least among sites $S_I$ and $S_{II}$.

## INTRODUCTION

The application of Raman spectroscopy to studies of adsorption on oxides and zeolites prior to 1975 has been reviewed (*1, 2*). In much of this work pyridine has been used as a probe molecule because some of the normal modes of vibration of the free pyridine molecule are perturbed and shifted in frequency in a predictable way depending on whether adsorption proceeds via physical adsorption, hydrogen-bonding, proton transfer (Brønsted acidity), or coordination to charge balancing cations or election-deficient Al atoms (Lewis acidity). For example, the symmetric ring breathing mode of pyridine ($\nu_1$) is a strong Raman scatterer and Raman studies of pyridine model compounds (*3, 4*) and of pyridine adsorbed on well-characterized solids has led to a fairly clear understanding of the behavior of this mode upon adsorption. Some of these results have been summarized in the review by Egerton and Hardin (*2*). Briefly, one can say that there are fairly clear domains for physisorption (991 $cm^{-1}$), hydrogen bonding (994–1008 $cm^{-1}$), Brønsted acidity (1009–1012 $cm^{-1}$), and Lewis acidity (1016–1025 $cm^{-1}$) for this ring mode. Egerton *et al.* (*3*) reported a Raman study of pyridine adsorption on seven cation exchanged Y zeolites. In agreement with Ward's (*5*) previous infrared results for similar systems, Egerton *et al.* (*3*) concluded from their Raman studies that for zeolite Y, pyridine adsorbs mainly to the cations. A linear correlation between the $\nu_1$ mode of pyridine and the electrostatic potential of the particular cation-framework pair was observed.

In this paper results are described for pyridine adsorption onto a sodium X zeolite, on nine cation-exchanged zeolites and on a decationated X zeolite as studied by Raman spectroscopy. The spectra of some metal nitrates dissolved in pyridine–nitromethane solutions were also obtained in order to examine whether cation electrostatic effects could be responsible for spectral variations as a function of exchange cation in the zeolites. Finally, the results are compared with those obtained by Freeman and Unland (*6*) for benzene adsorption on some X zeolites, and by Tam and Cooney (*4*) for pyrazine adsorbed on some alkali and alkaline earth-exchanged X zeolites.

[1] To whom enquiries should be directed. Present address: Syncrude Canada Ltd., Research Dept., P.O. Box 5790, Edmonton, Alberta, Canada, T6C 4G3.



0021-9517/80/040316-13$02.00/0

## EXPERIMENTAL

A Linde sodium 13X zeolite (NaX100) was used as a starting material for preparation of the ion-exchanged zeolites. The NaX100 zeolite was analyzed and had the composition $Na_{86}$ $(AlO_2)_{86}$ · $(SiO_2)_{106}$ · $264H_2O$ and a $Si^{4+}$ to $Al^{3+}$ ratio of 1.23 : 1. Partial exchange of $Na^+$ for $NH_4^+$, $Cs^+$, $K^+$, $Li^+$, $Pb^{2+}$, $Cd^{2+}$, $Zn^{2+}$, $Co^{2+}$, and $Ni^{2+}$ was accomplished by the method of Egerton *et al.* (*7*). The zeolites were analyzed by dissolution in perchloric and hydrofluoric acids followed by atomic absorption; the Kjeldahl method was used for nitrogen analysis in the $NH_4^+$-exchanged zeolite. The results are shown in Table 1 and we have designated a partially exchanged zeolite (e.g., $Cs^+$) with the symbol CsNaX37 which means that 37 mole% of the $Na^+$ has been exchanged by $Cs^+$.

X-Ray diffraction (XRD) patterns were measured to assure there were no changes in crystal structure or loss of crystallinity. A 57.3-mm Debye–Sherrer camera and Co$K\alpha$ radiation were used. For most samples these patterns indicated crystalline zeolite solids with small variations in the Fd3m unit cell parameter. However, there were significant changes in line intensities for PbNaX85 and CdNaX85. In neither case could a clear correlation to the NaX pattern be established and the material is labeled as an unknown crystalline solid. For this work, however, we will assume the bulk of the observed bands arise from adsorption onto residual crystallites of structure similar to that of NaX100. It should be pointed out that the sample crystallinities were not checked by XRD after heating, neither in $O_2$ nor in vacuum. It may be that there was some structural collapse during dehydration and dehydroxylation. This may be of particular concern for HNaX (*8*) and for samples with divalent cations (*9, 10*), cases where hydrolysis could be expected to be important. However, it is to be emphasized that the temperature was raised very slowly, particularly in the temperature range where most of the water would be evolved.

The HNaX partially decationized sample was formed by heating a fresh portion of the $NH_4NaX$ zeolite in $O_2$ at 500°C for 20 hr. The sample temperature was carefully raised at 100°C $hr^{-1}$ in a stream of dry $O_2$ in order to dry the zeolite prior to decationization. It is assumed that the degree of cation exchange is the same as in $NH_4NaX48$, i.e., HNaX48, and infrared measurements confirmed that no $NH_4^+$ remained.

Prior to pyridine adsorption, 200 mg of zeolite X sample was pressed at 350 kg $cm^{-2}$ into a 12.7-mm-diameter disc. These

TABLE 1

Analytical Results for Cationic Contents of Parent and Exchanged Zeolites

| X | Total[a] (mole) | Percentage Na exchanged[b] | Percentage Na left[b] | Total wt% cations |
|---|---|---|---|---|
| CsNaX37 | 0.4034 | 37 | 53 | 90 |
| KNaX46 | 0.3916 | 46 | 42 | 88 |
| $NH_4NaX48$ | 0.3959 | 48 | 41 | 89 |
| NaX100 | 0.4489 | 0 | 100 | 100 |
| LiNaX51 | 0.4375 | 51 | 47 | 98 |
| PbNaX85 | 0.3821 | 85 | 2 | 87 |
| CdNa85 | 0.3950 | 85 | 3 | 88 |
| ZnNaX78 | 0.4575 | 78 | 23 | 101 |
| CoNaX78 | 0.4577 | 78 | 24 | 102 |
| NiNaX63 | 0.3914 | 63 | 24 | 87 |

[a] Sum of (No. of moles of Na) + ($n$ × No. of moles of metal) of charge $n^+$.

[b] Based on NaX100 containing 0.4489 moles per 100 g.

discs were pretreated in the spectroscopic cell by slowly heating from 20 to 200°C in a high-purity oxygen stream. The temperature was held at 200°C for 1 hr before being increased slowly to 325°C. After 5 hr at 325°C the sample temperature was raised to 500°C, where it was maintained for 16 hr.

This procedure was designed to reduce the fluorescence which has been reported in some Raman surface studies (*1–3*). Prior to pyridine adsorption, each sample was degassed for 1 hr at 330°C in a vacuum of $1 \times 10^{-5}$ Torr. However, $NH_4NaX48$ was only partially dehydrated, i.e., in vacuum at 100°C for 3 hr.

The spectroscopic cell was basically the same as previously described (*3*). The discs were cooled in the evacuated cell to room temperature before absorption of pridine. The adsorbate (reagent grade $C_5H_5N$) was degassed by several freeze-pump-thaw cycles before use. Adsorption of pyridine vapor proceeded volumetrically in equal steps of approximately 0.013 $cm^3\ g^{-1}$. After addition of more than 0.16 $cm^3\ g^{-1}$ of pyridine vapor, the samples were exposed to the saturated vapor pressure of pyridine.

Raman spectra were also obtained of alkali and transition metal nitrates dissolved in 1.5 *M* solutions of pyridine in nitromethane following the method of Rouvière *et al.*(*11*). For $LiNO_3$ regular liquid cells were used. For $Co(NO_3)_2$ and $Pb(NO_3)_2$ the samples were run using a Spex rotating liquid Raman cell. The metal nitrates dissolved only with difficulty and after agitating at 20°C for 18 hr.

Raman spectra were recorded at each stage of adsorption for pyridine in the region of the $\nu_1$ and $\nu_{12}$ in-plane ring vibration bands (980–1050 $cm^{-1}$). Other weaker pyridine bands in the 400–3200 $cm^{-1}$ region were usually recorded only for pyridine-saturated zeolites. Spectra were recorded with resolution of 4 $cm^{-1}$. Scan speeds were typically 5 $cm^{-1}\ min^{-1}$ with photon counting rates of 200–1000 cps on a background of up to 2000 cps. Band positions were calibrated with respect to nearby nonlasing emission lines (NLL) of the argon ion laser.

Raman scattering was provoked by the 488.0-nm line of an argon ion laser which irradiated the sample at near normal incidence. The laser beam was focused by a 50-cm focal length spherical lens onto a 5-cm focal length cylindrical lens. The resultant image on the sample was a 10-mm-long "pencil" of radiation. The power level measured at the sample without an interference filter was about 110 mW. Radiation scattered from the sample (which was inclined at 30° with respect to the vertical) was focused on the entrance slit of a Jarrel-Ash model 100-25 Czerny-Turner double monochromator. A cooled RCA model C31034A photomultiplier detector was used in conjunction with linear photon counting.

## RESULTS

There is an extensive literature describing the vibrational spectroscopy of pyridine and its adducts (*12, 13*). For the present it is sufficient to note that pyridine has a total of $10A_1$, $3A_2$, $5B_1$, and $9B_2$ normal modes under $C_{2v}$ symmetry. The $A_1$ and $B_1$ symmetry modes are basically in-plane vibrations while $A_2$ and $B_2$ are out-of-plane. The symmetry modes correspond very closely to those of benzene (*12a*) and for Raman studies the more polarizable $A_1$ modes should yield higher scattering intensities. The most intense of these are $\nu_1(A_1)$ (symmetric ring breathing, 991 $cm^{-1}$), $\nu_{12}(A_1)$ (symmetric ring deformation, 1030 $cm^{-1}$), and $\nu_2(A_1)$ (symmetric C–H stretch, 3055 $cm^{-1}$). Other observed modes are $\nu_{8a}$, $\nu_{8b}$ (symmetric and asymmetric ring deformation HCC bend; 1573, 1581 $cm^{-1}$), $\nu_{6a}$, $\nu_{6b}$ (symmetric and asymmetric ring deformation CCC bend; 604, 653 $cm^{-1}$), and $\nu_3$, $\nu_{9a}$ (totally symmetric HCC bend, symmetric HCCH bend; 1217 $cm^{-1}$).

The totally symmetric ($\nu_1$) ring breathing mode of pyridine near 1000 $cm^{-1}$ is most sensitive to changes in cations. The positions of this band for the 11 zeolites studied are shown in Table 2 and some spectra are shown in Fig. 1. Distinct $\nu_1$ doublets were

TABLE 2

The Positions and Bandwidths of Pyridine $\nu_1$ Bands[a]

| Exchange cation | $\nu_1(A_1)$[b] | | Exchange cation | $\nu_1(A_1)$ | |
|---|---|---|---|---|---|
| | $cm^{-1}$ | FWHM[c] $cm^{-1}$ | | $cm^{-1}$ | FWHM $cm^{-1}$ |
| $NH_4^+$ | 996 | 10 | $Pb^{2+}$ | 1004 | 14 |
| | ~1010 | sh | | 994 | — |
| | 1017 | 15 | | | |
| | | | $Cd^{2+}$ | 1013 | 11 |
| $H^+$ | 998 | 11 | | | |
| | | | $Zn^{2+}$ | 996 | 10 |
| $Cs^+$ | 991 | 10 | | 1017 | 12 |
| | 999 | sh | | | |
| $K^+$ | 994 | 12 | $Co^{2+}$ | 1017[d] | — |
| $Na^+$ | 997 | 9 | $Ni^{2+}$ | 997[d] | — |
| | | | | 1019[d] | — |
| $Li^+$ | 999 | 11 | | | |
| | 1007 | sh | Pyridine (*l*) | 991 | 7 |

[a] Dosage approximately 0.13 $cm^3\ g^{-1}$.
[b] Includes $\nu_1'$ and $\nu_1''$—see text.
[c] FWHM—full width at half maximum.
[d] Very weak at saturation.

observed for $NH_4NaX48$, ZnNaX78, and NiNaX63. (For reasons which will become apparent later, we have adopted the following convention for labeling the $\nu_1$ bands; $\nu_1$ designates a band due to an interaction between pyridine and an exchanged cation and $\nu_1'$ is for a pyridine $Na^+$ interaction when there is residual Na in the zeolite except for NaX100 where it is designated as $\nu_1$.) For Ni and Co the $\nu_1$ Raman signals were exceptionally weak, and other bands were observed with difficulty. However, the CoX sample was dark blue, as expected, whereas the faintly pink NiX sample turned blue upon irradiation by the laser when pyridine was present (see below). The remaining samples were white except for CsX which was pale pink at near saturation.

The $\nu_1$ and $\nu_{12}$ Raman band positions and relative peak heights for the metal nitrates dissolved in 1.5 *M* pyridine/nitromethane solutions are shown in Table 3 along with values for the solution itself.

The position and relative peak heights of all Raman bands observed for four group IA cation exchanged NaX zeolites and for $NH_4NaX48$, decationized HNaX48, PbNaX85 and ZnNaX78 zeolites are reported in Table 4. The data are for pyridine coverage of 0.13 $cm^3\ g^{-1}$. Only the $\nu_1$ bands were observed for CdNaX85 (1013 $cm^{-1}$) and CoNaX78 (1017 $cm^{-1}$). For NiNaX63, at saturation, bands were observed only at 3073, 1016, and 997 $cm^{-1}$.

## DISCUSSION

The results are discussed first in terms of the ratio of exchange cation to residual sodium cation, the total moles of cations per unit cell, and the interactions of pyridine molecules with cations in the supercages. The general features of the Raman spectra are then discussed mainly in terms of the position of the $\nu_1$ band of adsorbed pyridine for different exchanged cations. By analogy with the works of Pickert *et al.* (*14*), Ward (*5a*), and Dempsey (*15*), correlations are drawn between the shift of $\nu_1$ and the electrostatic potential of (a) an interacting cation in some pyridine–metal nitrate–nitromethane solutions, and (b) the cations in the exchanged zeolites.

### *a. Cation Exchange*

An effect of our exchange procedure can be seen in Table 1. Exchanges for $Li^+$, $Zn^{2+}$, and $Co^{2+}$ gave virtually all of the expected 86 cationic equivalents per unit cell. However, exchanges for $Cs^+$, $K^+$, $NH_4^+$, $Pb^{2+}$, $Cd^{2+}$, and $Ni^{2+}$ gave only 85–90% of the total expected 86 cations. The latter may be due to leaching during the wash steps.

There are two main sets of samples to be considered in terms of the ratio of exchange cation (M) to residual sodium: (a) those having 45–50% exchange (K, $NH_4$, Li) and, (b) those having 78–85% exchange (Pb, Cd, Zn, Co). Two samples are unique: $Cs^+$ (37%) and $Ni^{2+}$ (63%). We will assume a statistical distribution of group I cations among the $S_I$, $S_{II}$, and $S_{III}$ sites (*16*) except for the larger $Cs^+$ which would be expected to occupy only the $S_{II}$ and perhaps $S_{III}$ sites. The possible site distribution for the transition metal ions will be discussed after the Raman results.

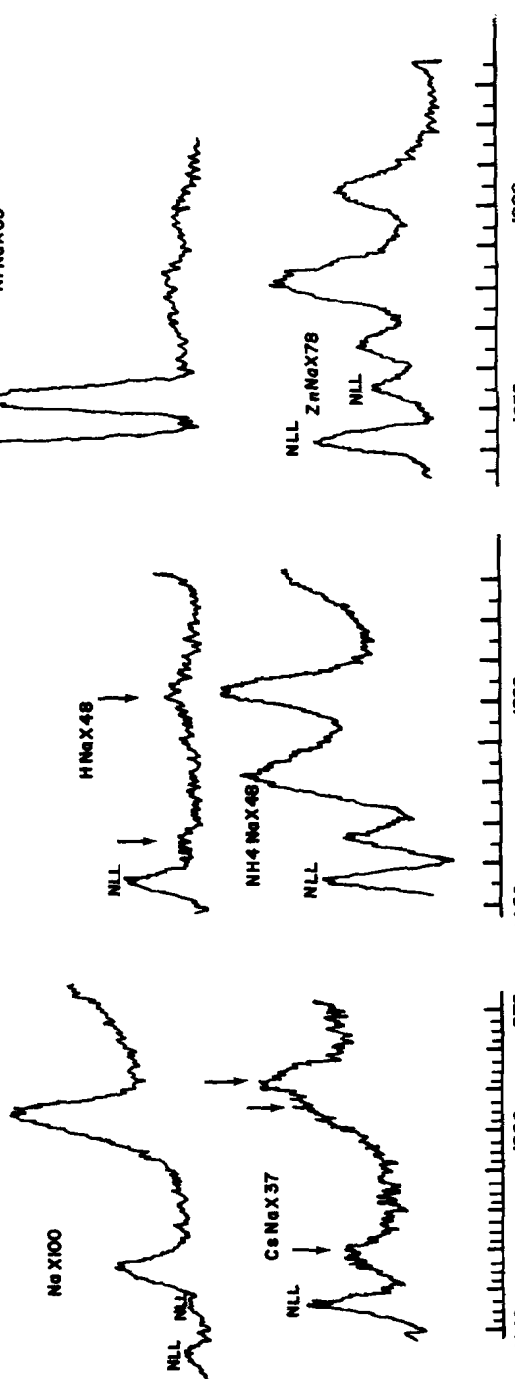


FIG. 1. Raman spectra observed in the $\nu_1$ and $\nu_{12}$ regions of pyridine absorbed on a series of partially cation-exchanged X zeolites. These spectra were recorded, after equilibration, at pyridine dosing equivalent to 0.13 $cm^3\ g^{-1}$.

TABLE 3

The $\nu_1$ and $\nu_{12}$ Raman Bands of Pyridine–Metal Nitrite–Nitromethane Solutions[a]

| | Pyridine/ nitromethane (1.5 M) | | $KNO_3$/PNM[b] | | $NaNO_3$/PNM | | $LiNO_3$PNM | |
|---|---|---|---|---|---|---|---|---|
| | $cm^{-1}$ | RPH | $cm^{-1}$ | RPH | $cm^{-1}$ | RPH | $cm^{-1}$ | RPH |
| $\nu_{12}$ | 1031 | 70 | 1031 | 70 | 1030 | 74 | 1032 | 91 |
| $\nu_{1a}$ | — | — | 996 | ws[c] | 997 | ws | 1004 | 66 |
| $\nu_{1b}$ | — | — | — | — | — | — | — | — |
| $\nu_1$ | 991 | 10 | 991 | 10 | 989.5 | 10 | 992 | 10 |

| | $Pb(NO_3)_2$/PNM | | $Cd(NO_3)_2$/PNM | | $Co(NO_3)_2$/PNM | | $Ni(NO_3)_2$PNM | |
|---|---|---|---|---|---|---|---|---|
| | $cm^{-1}$ | RPH | $cm^{-1}$ | RPH | $cm^{-1}$ | RPH | $cm^{-1}$ | RPH |
| $\nu_{12}$ | 1031 | 93 | 1030.5 | 78 | 1031.3 | 81 | 1031.5 | 10.8 |
| $\nu_{1a}$ | 1003.5 | 3.5 | 1010.5 | 44 | 1013 | 1.9 | 1015 | 10.7 |
| $\nu_{1b}$ | — | — | 996 | 22 | — | — | 998.5 | 7.1 |
| $\nu_1$ | 991 | 10 | 990 | 10 | 990.7 | 10 | 990.5 | 10 |

[a] $\nu_1$ = free pyridine; $\nu_{1a}$ = metal-coordinated pyridine; $\nu_{1b}$ = H-bonded.
[b] PNM = 1.5 M pyridine in nitromethane.
[c] ws = weak shoulder.

### b. *Raman Spectra*

Considering the possible variations in interaction energies for pyridine adsorbed at different sites or by different mechanisms one might expect detectable variations in band widths and peak positions for increasing dosage. In this work no significant variations of band widths were observed as a function of coverage (see Fig. 2 for LiNaX). Further, the peak positions varied by not more than $\pm 2$ $cm^{-1}$ for coverages from 0.013 $cm^3 g^{-1}$ to saturation (>0.16 $cm^3 g^{-1}$). In view of the relatively large slit widths used, 4 $cm^{-1}$, these variations in peak position are felt to be insignificant.

TABLE 4

Raman Bands from Pyridine on Ion Exchanged X Zeolites

| Normal mode, $\nu$ | Position in $cm^{-1}$ (relative peak height) | | | | | | | | |
|---|---|---|---|---|---|---|---|---|---|
| | Py (*l*) | Cs[a] | K | Na | Li[b] | $NH_4$[c] | H | Pb | Zn |
| 20b | 3089(4) | | | | | | | | |
| 2, 13 | 3055(52) | 3059(330) | | 3061(68) | | 3065(120) | | 3069(174) | 3068(257) |
| 8a | 1581(6) | 1635(60) | | 1591(10) | 1591(12) | 1623(5) | | 1599(39) | 1610(8) |
| 8b | 1573(6) | 1588(70) | | 1570(9) | 1570(12) | 1586(5) | | | 1593[d] |
| 3, 9 | 1217(8) | 1203(45) | | 1210(11) | 1223(15) | 1212(19) | | 1233(15)[d] | 1223(19) |
| 12 | 1030(81) | 1031(77) | 1033(67) | 1035(54) | 1036(56) | 1032(53) | 1034(63) | 1034(174) | 1033(45) |
| 1 | 991(100) | 990(100) | 994(100) | 997(100) | 999(100) | 996(100) | 998(100) | 1004(100) | 1017(100) |
| 1′ | | 996(sh) | | | | 996(100) | 998(100) | 994(40)[d] | 996(61) |
| 6b | 653(8) | 651(40) | 653(40) | 650(12) | 650(24) | 651(18)[d] | 650(63) | 651(43) | 652(19) |
| 6a | 604(3) | 607(25) | | 616(5) | 613(4) | 608(5)[d] | | | |

[a] Bands also at 1308(65), 1352(65), 1436(50), and 1514(50) $cm^{-1}$.
[b] Unassigned weak shoulder at 1007 $cm^{-1}$.
[c] Bands also at 1400(6), 1017(100), and 1010(sh) $cm^{-1}$.
[d] Only observed at saturation. The other data is for a dosage of 0.13 $cm^3 g^{-1}$.

*Group IA cations.* The Raman spectra of pyridine (py) adsorbed on X zeolites with $K^+$, $Na^+$, and $Li^+$ cations have no unusual features (Fig. 1). The main diagnostic band, $\nu_1$, shifts in a regular manner as the cations change (Table 4). Following the work of Ward (*5, 9*), one assigns this to py–cation coordination effects. The remaining bands, for NaX100 at least, are subjected to more moderate shifts. However, one can separate the bands into two groups: (a) the $B_1$ modes shifting down by 3–7 $cm^{-1}$ from their corresponding values in liquid pyridine; (b) the $A_1$ modes shifted up by 5–10 $cm^{-1}$. As had been demonstrated by Cooney *et al.* (*17*) the intensity of the Raman bands can be used to measure a form of adsorption isotherm. In Fig. 3 we have shown a simplified version of this which, nonetheless, clearly demonstrates the type II adsorption behavior of pyridine in NaX100. The pore volume of the supercages has been found to be 0.30 $cm^3\ g^{-1}$ or five molecules per cage for benzene (*16*). In Fig. 3 the first break, near 100 cps, corresponds to approximately 0.5 molecules of pyridine per supercage. The break upward near 125 cps corresponds to about 1 molecule per supercage and the plateau at ~250 cps corresponds to about two pyridine molecules added per supercage. Exposure of the NaX100 sample to the equilibrium vapor pressure of pyridine for extended periods did not significantly change the peak heights detected. This apparent minimum may be caused by localized desorption under the heating effect of the laser beam.

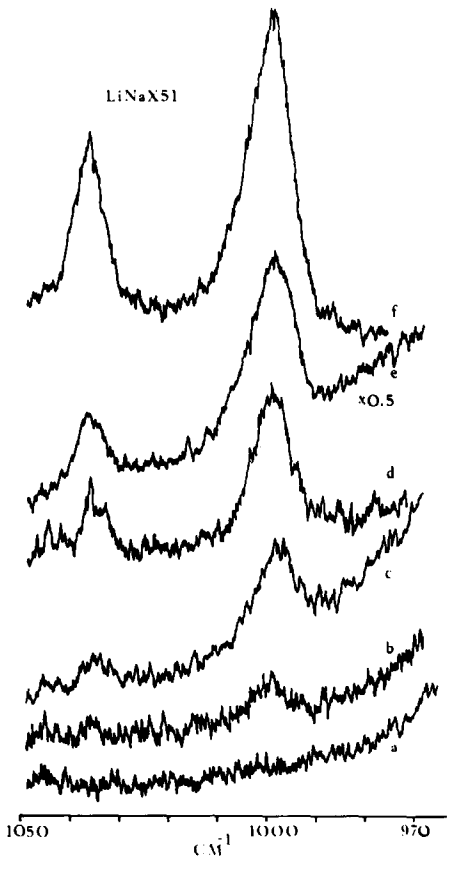


FIG. 2. Raman spectra of the $\nu_1$ and $\nu_{12}$ bands of pyridine adsorbed on LiNaX51 as a function of dosage ($cm^3\ g^{-1}$): (a) 0.003, (b) 0.006, (c) 0.013, (d) 0.026, (e) 0.051, (f) 0.13. Due to changes in sample position between doses, intensity comparisons between different spectra are not meaningful.

The data obtained for CsNaX37 are unusual in three respects: four extra bands were observed, the sample was pink at saturation pyridine coverage, and the relative peak heights (with respect to $\nu_1$) are accentuated as compared to the other zeolites (Table 4). The $\nu_1$ band observed at 991 $cm^{-1}$ is assigned to pyridine coordinated to $Cs^+$ in the supercages whereas the $\nu_1$ shoulder at 999 $cm^{-1}$ is assigned to pyridine coordinating to residual $Na^+$ cations. The significant shifts up for $\nu_{8a}$ and $\nu_{8b}$, +54 and +15 $cm^{-1}$, respectively (Table 4), are similar to those observed for the $NH_4NaX48$ sample discussed below. Analysis for total cations indicated a 10% deficiency. Hence some lattice hydrolysis may have occurred, giving some potential Brønsted acid sites. Evacuation at 500°C would thus be expected to create some structural defects, and possible Lewis acidity [Breck schemes II and III (*16*)]. However, unlike $NH_4NaX48$ the values of 1635 $cm^{-1}$ and 1588 $cm^{-1}$ do not correlate well with any of the hydrogen bonding, Lewis acid, Brønsted acid, or physisorption models.

An alternative explanation may be found in considering the pink color of the sample

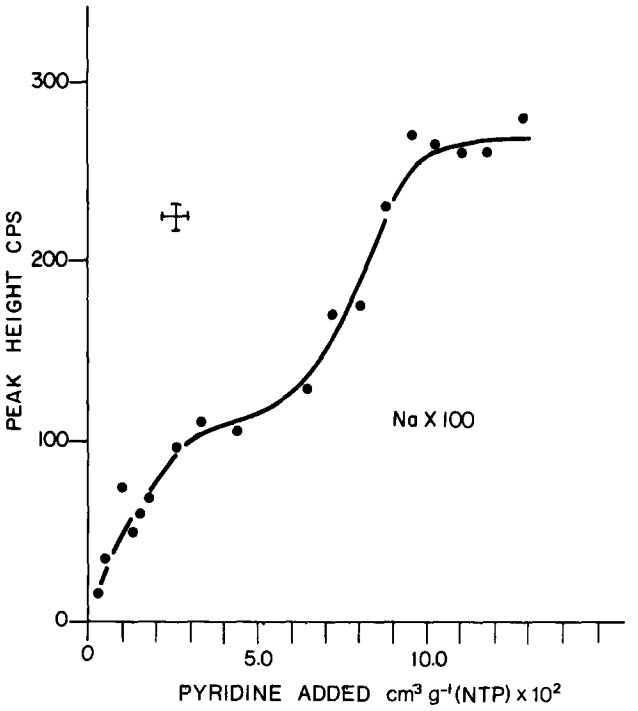


FIG. 3. The growth in the peak height of the $\nu_1$ Raman band (near 1000 $cm^{-1}$) for pyridine absorbed onto NaX100. The values were taken from spectra recorded within 30 min of addition of the respective doses of pyridine. The probable limits of error are indicated.

at saturation. We propose that this color arises from the formation of $Cs_6^{5+}$ or $Cs_4^{3+}$ species by photoreduction of the cation with resultant formation of some (pyridine)$^{+1}$. The existence of pink NaY after $\gamma$-irradiation was previously explained, using ESR data, on the basis of an electron trap color center (*18*). An electron trapped in a sodalite cage and shared by four sodium ions at site II was proposed. The broad red absorption band near 500.0 nm corresponds to a transition from ground state to first excited state for an electron-in-a-box having an edge of approximately 0.67 nm. The four sites II in zeolite X are separated by approximately 0.6 nm (*18*). Similar species were proposed for samples of NaY exposed to Na vapor above 300°C and for NaX exposed to Na vapor (*19*). Therefore, the large changes in intensities of all the pyridine Raman bands for the CsNaX37 case, as well as the extra bands, may be attributable to the formation of $Cs_Y^{(X-1)+}$ and (pyridine)$^{+1}$ species. A precedent for the additional Raman bands can be found in some earlier work for pyridine adsorption on bentonite clay (*20*).

*Transition metal cations.* The divalent cation samples CdNaX85 and CoNaX78 gave only very weak spectra. In fact only $\nu_1$ was observed in either case (Table 2). For CdNaX85 the general background light level was approximately 100 times as intense as for the strongest Raman band observed, which limited the detectability of the weaker Raman bands. Assuming pyridine is adsorbed at zeolite X crystallites (see X-ray result) then the band observed at 1013 $cm^{-1}$ is assigned to pyridine coordinated with $Cd^{2+}$.

The CoNaX78 sample was dark blue after evacuation at 500°C. The presence of strongly absorbing visible electronic transition bands severely limits the degree of Raman scattering in this case. The very low background level of 5–10 cps was approximately 20 times less than for other white zeolites. The weak Raman band observed

at 1017 $cm^{-1}$, for a coverage of about 0.20 $cm^3 g^{-1}$, is assigned to $\nu_1$ of pyridine coordinated to $Co^{2+}$. The anhydrous NiX63 sample was greyish after evacuation at 500°C and turned faintly pink when pyridine was added. At moderate coverage (0.15 $cm^3 g^{-1}$) only one weak band was observed at 1019 $cm^{-1}$ which has been assigned to $Ni^{2+}$–pyridine interaction, whereas at saturation an additional band at 997 $cm^{-1}$ appeared which could be due to $Na^+$–pyridine. At low coverage (0.013 to 0.10 $cm^3 g^{-1}$) a blue spot formed upon irradiation by the laser. This did not occur at higher coverages and might account for our failure to detect Raman scattering at low coverage. The pinkish $Ni^{2+}$ ion has a broad electronic absorption band between 450 and 500 nm (*21*) and we can speculate that photoreduction might be possible at low coverage leading to the formation of a colored $Ni^+$–pyridine$^+$ complex.

The Raman results for the crystalline ZnNaX78 (Fig. 1 and Table 4) show that relatively intense and well-defined bands were obtained even at low coverage. As in all the above cases, bands at 1017 and 996 $cm^{-1}$ were assigned to $\nu_1$ and $\nu_1'$ of pyridine molecules coupled to $Zn^{2+}$ and $Na^+$, respectively.

PbNaX85 gave a good, crystalline XRD pattern, however the structure was unknown. Assuming that some zeolite structure was retained and that this accounted for the bulk of the adsorption sites, we assign the Raman bands at 1004 $cm^{-1}$ to $\nu_1$ for py–$Pb^{2+}$. The additional weak band at 994 was only observed at saturation and is probably due to liquid-like pyridine.

*Ammonium and decationated.* The spectra from HNaX48 were very weak even at high coverage (Fig. 1) and few bands were detected (Table 4). The weakness of the bands is consistent with some structural collapse and loss of sites as found by Ward (*22*) for heating above 480C (500°C here). Consequently only traces of residual $NH_4^+$ would be expected as well as initiation of dehydroxylation with associated structural collapse (*16, 22*), i.e., scheme 7 of Breck. The Raman band observed near 998 $cm^{-1}$ is consistent with $\nu_1$ of pyridine hydrogen bonded to structural OH groups. However, it is also consistent with coordination to $Na^+$. There was no evidence for Lewis (1017 $cm^{-1}$) or Brønsted (1010 $cm^{-1}$) sites (*2*).

As a result of the method of pretreatment of the $NH_4$NaX48 sample, i.e., heating in vacuum at 110°C for 3 hr, it would be expected to contain residual $H_2O$ (*16*, pp. 4–11), to have had some $NH_4^+$ decomposition (*8*) and to have some structural OH groups (*23*) at O(*2*) and O(*3*) near sites II, I′, and I (*24*). Thus, there are expected to be sites for: (a) pyridine coordination to $NH_4^+$ and $Na^+$ cations; (b) pyridine hydrogen bonding to residual $H_2O$; and (c) formation of pyridinium ions at sufficiently acidic Brønsted sites. The formation of Lewis acid sites would not be consistent with the low temperature of treatment or the presence of residual $H_2O$.

The dominant Raman bands for pyridine adsorbed on $NH_4$NaX48 are shown in Fig. 1 and the values for all observed bands are given in Table 4. The extra band observed at 1400 $cm^{-1}$ is almost certainly due to $\nu_4$ ($F_2$) of $NH_4^+$ which is also observed at 1400 $cm^{-1}$ for ammonium halides (*25*). The strength of the Raman band observed here at 3065 $cm^{-1}$ may be partly attributable to $\nu_1(A_1)$ of $NH_4^+$ reported to be at 3040 $cm^{-1}$ (*25*).

The band at 1017 $cm^{-1}$ is broad and asymmetric on the low wavenumber side (Fig. 1). Part of this may be due to a weaker, underlying band near 1010 $cm^{-1}$ due to Brønsted acidity and the formation of pyridinium ions. By comparison with other zeolites in this work and elsewhere (*3*) and by comparison to model compounds (*2*) one would assign the 1017 $cm^{-1}$ band to a pyridine–$(NH_4)^+$ coordination complex. However, based on plots of $\nu_1$ vs $e/r$ (see below) one would infer an ionic radius of approximately 0.033 nm, far too small for $NH_4^+$ (0.148 nm). A band at 1017

$cm^{-1}$ is also consistent with Lewis acid coordination, for example, to structural defects (*2*). However, such a model seems unlikely in view of the water present. A more probable assignment appears to be a shifted $\nu_1$ arising from either pyridinium ions formed at Brønsted sites or pyridine strongly hydrogen bonded to $H_2O$ or OH groups. The presence of bands near 1623 and 1586 $cm^{-1}$ supports the presence of hydrogen bonded species (*8*, p. 226). The band observed at 996 $cm^{-1}$ can be attributed to $\nu_1$ of pyridine coordinated to residual $Na^+$ or to undissociated $NH_4^+$. Rouvière *et al.* (*11*) report a band at 1002 $cm^{-1}$ for $NH_4SCN$ in a 1.5 *M* pyridium in nitromethane solution.

### c. *Model Systems and Electrostatic Potential*

Physical models used to interpret both the infrared (*5, 9, 22*) and Raman (*3*) results for pyridine sorption in zeolites have been based on direct coupling of pyridine to the charge balancing cations. A simple chemical analog to this can be found in the solutions of metal nitrates in a solution of pyridine in nitromethane. Following the work of Rouvière *et al.* (*11*), concentrated solutions of metal nitrates were prepared in a 1.5 *M* pyridine in nitromethane solution (Table 3). The concentration of the metal nitrates varied, giving rise to potential differences in solvation number for pyridine around the cations (*11*). Thus, the relative intensities of the "free" $\nu_1$ and "coupled" $\nu_1$ bands should not be compared.

If one assumes, as for zeolites, that the local electrostatic potential is proportional to the charge-to-radius ratio of the cations then one can plot $\nu_1(A_1)$ vs $e/r$, after Ward (*5, 9, 22*) and Egerton *et al.* (*3*) (Fig. 4). Here we have plotted only the main perturbed $\nu_1$ peak, i.e., $\nu_{1a}$. There is a fairly well-behaved linear correlation that extrapolates to "zero" potential at 991 $cm^{-1}$ for the undoped 1.5 *M* pyridine–nitromethane solution. No such correlation was observed for $\nu_{12}(A_1)$.

In all cases the "free," or noncation associated, pyridine gave rise to $\nu_1$ near 991 $cm^{-1}$. As well, in some cases a third band was observed in this region, $\nu_{1b}$ (Table 3). This is most probably due to pyridine hydrogen bonded to $H_2O$ entrained in the

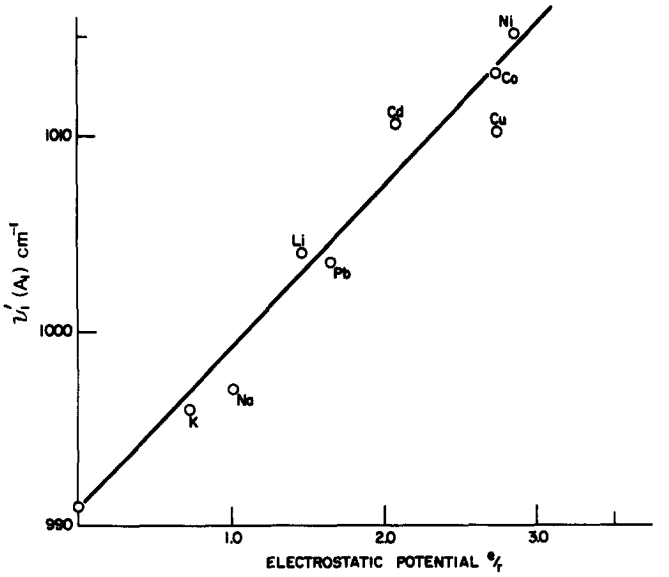


FIG. 4. Pyridine–nitromethane solutions of metal nitrates. A plot of the pyridine $\nu_{1a}$ mode vs the cationic charge-to-radius ratio, $e/r$.

sample as residual water of hydration from the metal nitrates, i.e., $Cd(NO_3)_2$/PNM and $Ni(NO_3)_2$/PNM with bands at 996 and 998.5 $cm^{-1}$, respectively (Table 3).

A plot of the $\nu_1$ band positions which have been assigned to a cation–pyridine interaction against $e/r$ for zeolite X is given in Fig. 5. In spite of obvious differences which would be expected in considering the electrostatic potential in a liquid solution as opposed to a crystalline zeolite, it is most satisfactory to find that the linear correlation for the zeolites was as good as that shown above for the nitromethane solutions. We believe that this confirms our assignments for the $\nu_1$ modes (Table 4). A similar $\nu_1$ vs $e/r$ correlation was found for the Y zeolites (*3*), and Ward has also made use of these plots with respect to the 1440 $cm^{-1}$ band of pyridine in his infrared work (*5, 9, 22*). As was found with the PNM solutions, and for zeolite Y, no such correlation was found for the $\nu_{12}$ band.

It should be noted that the observed frequency for the $\nu_1$ mode for the LiNaX51 is lower than predicted in the plot of frequency vs $e/r$. Ward (*22*) also found a similar deviation in the plot of hydroxyl frequencies vs $e/r$ for alkali-exchanged Y zeolites and assumed that the assumptions made in calculating the electrostatic potential (*26*) may not be applicable for small cations. This was also true with respect to the 1440 $cm^{-1}$ band ($\nu_{19b}$) of pyridine coordinated to alkali-exchanged Y zeolites (*5a*) and to a lesser extent this was also true for $\nu_1$ in the Raman spectrum of pyridine adsorbed on a LiY zeolite (*3*).

The band position for CsNaX is also lower than predicted by the line in Fig. 5. This might be associated with the earlier mentioned partial reduction of Cs, i.e., $Cs_6^{5+}$, in which case the average charge per cesium ion would be less than +1. If this was correct, then the point for CsNaX in Fig. 5 would shift to lower $e/r$, i.e., toward the line.

Most of the exchanged X zeolites had residual $Na^+$ and Raman bands due to a pyridine–Na interaction have been designated $\nu_1$, in Table 4. The frequencies, as expected, are all very close to that observed for NaX100, and would correspond to a nearly horizontal line if plotted vs $e/r$($r$ of the exchanged cation) in Fig. 5. Finally, the two strong bands observed for the $NH_4^+$-exchanged zeolite are also plotted in Fig. 5, and it can clearly be seen that it

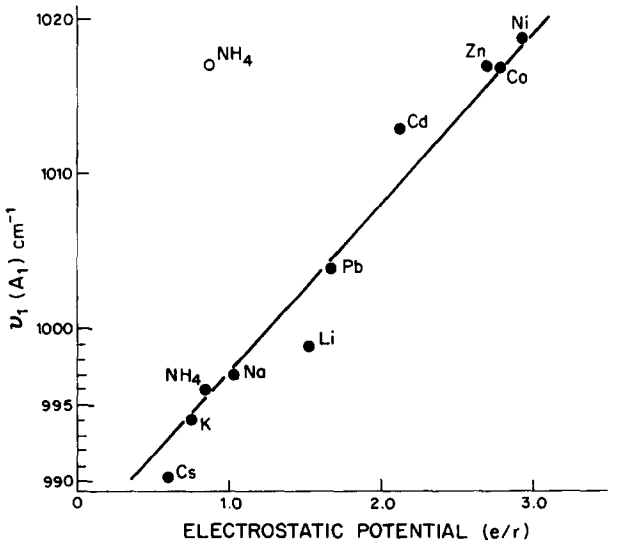


FIG. 5. Plot of the $\nu_1$ Raman band of pyridine adsorbed on X zeolites as a function of the charge-to-radius of the exchanged cation.

would be unreasonable to assign the 1017 $cm^{-1}$ band to a specific $NH_4^+$–pyridine interaction.

*d. Comparison of X and Y*

Comparison of the results from NaX100 and LiNaX51 with those from NaY100 and LiNaY70 shows *no* marked changes in band positions or intensities (Table 5). In the examples of Li exchange the largest shift was 3 $cm^{-1}$ (X to Y) and this may be attributed to larger electrostatic fields in Y vs X or variations in spectrometric accuracy. However, six of the eight $A_1$ and $B_1$ in-plane modes of NaY100 are 4 to 9 $cm^{-1}$ higher than their NaX100 analogs. In comparison to liquid pyridine the $B_1$ modes are less perturbed than the $A_1$ modes. This can be interpreted to indicate a stronger perturbation of the $\pi$ electrons of pyridine in Y as opposed to X. This perturbation is probably an indirect consequence of cation–pyridine coordination rather than a result of the cation directly perturbing the $\pi$ electron system of the ring. Freeman and Unland (*6*) recently studied the Raman spectra of benzene adsorbed on a series of alkali-exchanged X and Y zeolites and in all cases the $\nu_1$ band of benzene was shifted to lower frequency relative to $\nu_1$ of pure benzene and they suggested that the $\pi$ electron system of benzene was interacting with the cation. In our case, all shifts of $\nu_1$ of pyridine were to higher frequency (except for $Cs^+$) and followed the trend for the pyridine/nitromethane solutions. Thus, pyridine interacts with the cations via a direct $C_5H_5N: \rightarrow M^+$ coordination mechanism whereas benzene, lacking the lone pair of electrons, can probably only interact via a $\pi$–$M^+$ mechanism.

TABLE 5

Raman Bands for Pyridine Adsorbed on Zeolites 13X and 13Y

| | Raman band ($cm^{-1}$) | | | | |
|---|---|---|---|---|---|
| | Liquid | NaX100 | NaY100 | LiNaX | NiNaY |
| $\nu_{8a}(A_1)$ | 604 | 616 | 613 | 613 | — |
| $\nu_{9b}(B_1)$ | 653 | 650 | 654 | 650 | 651 |
| $\nu_1(A_1)$ | 991 | 997 | 1002 | 999 | 1002 |
| $\nu_{12}(A_1)$ | 1030 | 1035 | 1036 | 1036 | 1036 |
| $\nu_{3,9a}(B_1, A_1)$ | 1217 | 1210 | 1218 | 1223 | 1223 |
| $\nu_{8b}(B_1)$ | 1573 | 1570 | 1574 | 1570 | — |
| $\nu_{8a}(A_1)$ | 1581 | 1591 | 1596 | 1591 | 1594 |
| $\nu_{2,13}(A_1)$ | 3055 | 3061 | 3070 | — | 3063 |
| $\nu_{20}(B_1)$ | 3089 | — | — | — | — |

The most marked difference in the Raman spectra for X and Y zeolites was the observation of two $\nu_1$ pyridine bands for most cation-exchanged X zeolites and one $\nu_1$ band for Y zeolites. The observation of the $\nu_1$ band due to a pyridine–$Na^+$ interaction only for the exchanged zeolites may be attributable in some cases to the greater number of cations in the supercages of X and Y. For the alkali-exchanged X zeolites (37–51% exchange) we expect and observe two $\nu_1$ bands except for $K^+$ where $\nu_1$ are presumably too close to be resolved. For $Pb^{2+}$ and $Cd^{2+}$ analysis indicated (Table 1) essentially no residual $Na^+$ and only one $\nu_1$ band was observed at less than saturation. Each of the $Zn^{2+}$, $Ni^{2+}$, and $Co^{2+}$-exchanged X zeolites had about 24% residual $Na^+$, and the expected $\nu_1$ and $\nu_1'$ was observed only for $Zn^{2+}$ and $Ni^{2+}$. However, the $Co^{2+}$ zeolite was dark blue and a $\nu_1$ band having an extremely poor signal-to-noise ratio was observed only at near saturation coverage, and a weaker $\nu_1'$ band could conceivably have been lost in the background noise.

According to Rabo *et al.* (*26*), bivalent cations preferentially exchange with $S_I$ $Na^+$ ions, and in terms of the percentage residual $Na^+$ in the $Zn^{2+}$, $Ni^{2+}$, and $Co^{2+}$ samples, most of the $Na^+$ should therefore be at $S_{II}$ and $S_{III}$ with $M^{2+}$ at $S_I$. However, an $M^{2+}$ ion at $S_I$ should be inaccessible to pyridine lone pair interactions. In view of the fact that the Raman spectra clearly showed that a $M^{2+}$–pyridine interaction existed (under our experimental conditions) we assume that the $M^{2+}$ ions are distributed among $S_I$ and $S_{II}$ sites at least, as expected (*26*).

Finally, Tam and Cooney (*4*) have studied the Raman spectrum of pyrazine (1,4-diazine) adsorbed on some alkali and alka-

line earth-exchanged X zeolites and found that the perturbation of the symmetric ring breathing mode ($\nu_1$) was proportional to $r$ of the cation and was independent of the cation charge. This contrasts with our $e/r$ correlation for pyridine on X zeolites, and a similar correlation found by Ward (*22*) for pyridine ($\nu_{19b}$) on Y zeolites and by Egerton *et al.* (*3*) for $\nu_1$ of pyridine on Y. As noted by Tam and Cooney (*4*) pyrazine is a much weaker base than pyridine and, as it also has no dipole moment, it is reasonable that the mode of interaction with a cationic zeolite could be different for each molecule in that pyrazine would be less susceptible to accommodating positive charge than pyridine.

## ACKNOWLEDGMENTS

Financial support for this work was provided by the Water Resources Research Program of Environment Canada and by the National Research Council of Canada.

## REFERENCES

1. Cooney, R. P., Curthoys, G., and Nguyen The Tam. *Adv. Catal.* **24,** 293 (1975).
2. Egerton, T. A., and Hardin, A. H., *Catal. Rev. Sci.-Eng.* **11,** 1 (1975).
3. Egerton, T. A., Hardin, A. H., and Sheppard, N., *Canad. J. Chem.* **54,** 586 (1976).
4. Nguyen The Tam, and Cooney, R. P., *J. Chem. Soc. Faraday I* **72,** 2598 (1976).
5. (a) Ward, J. W., *J. Catal.* **10,** 34 (1968). (b) Ward, J. W., *J. Colloid Sci.* **28,** 269 (1968).
6. Freeman, J. J., and Unland, M. L., *J. Catal.* **54,** 183 (1978).
7. Egerton, T. A., and Stone, F. S., *J. Chem. Soc. Faraday Trans. I* **69,** 22 (1973).
8. Ward, J. W., "Zeolite Chemistry and Catalysts" (J. A. Rabo, Ed.), p. 142. ACS Monograph 171, 1976.
9. Ward, J. W., "Molecular Sieve Zeolites-I," 380. ACS Advances in Chemistry Series, No. 101, 1971.
10. Ward, J. W., *J. Phys. Chem.* **72,** 4211 (1968).
11. Rouvière, J., Dimou, B., Bron, B., and Salvinien, J., *C.R. Acad. Sci. Paris* **274C,** 458 (1972).
12. (a) Kline, C. H., and Turkevich, J., *J. Chem. Phys.* **12,** 300 (1944); (b) Corrsin, L., Fox, B. J., and Lord, R. C., *J. Phys. Chem.* **21,** 1170 (1953); (c) Miliceu, S., *J. Molec. Struct.* **25,** 189 (1975).
13. Wilmhurst, J. K., and Bernstein, H. J., *Canad. J. Chem.* **35,** 1883 (1957).
14. Pickert, P. E., Rabo, J. A., Dempsey, E., and Schomaker, V., *Proc. 3rd Int. Cong. Catal.*, Amsterdam, 1964.
15. Dempsey, E., "Molecular Sieves." Soc. Chem. Industry, London, 1968.
16. Breck, D. W., "Zeolites and Molecular Sieves," p. 96. Wiley-Interscience,, New York, 1974.
17. Cooney, R. P., and Nguyen The Tam, *Aust. J. Chem.* **29,** 507 (1976).
18. Kasai, P. H., *J. Chem. Phys.* **43,** 3322 (1965).
19. Kasai, P. H., and Bishop, R. J., "Zeolite Chemistry and Catalysis" (J. A. Rabo, Ed.), p. 382. ACS Monograph No. 171, 1976.
20. Davis, A. R., and Hardin, A. H., *Canad. J. Spect.* **21,** 139 (1976).
21. Polák, R., and Klier, K., *J. Phys. Chem. Solids* **30,** 2231 (1969).
22. Ward. J. W., *J. Catal.* **14,** 365 (1969).
23. Barthomeuf, D., "Molecular Sieves-II" (J. R. Katzer, Ed.), p. 453. No. 40, ACS Symposium Series, 1977.
24. Smith, J. V., "Zeolite Chemistry and Catalysis" (J. A. Rabo, Ed.), p. 37. ACS Monograph 171, 1976.
25. Nakamoto, K., "Infrared Spectra of Inorganic and Coordination Compounds," 2nd ed. Wiley, New York, 1976.
26. Rabo, J. A., Angell, C. L., Kasai, P. H., and Schomaker, V., *Trans. Faraday Soc.* **41,** 328 (1966).